Inorg. Chem. **2005**, *44*, 6536–6544

Discrete Iridium Pyridonate Chains with Variable Metal Valence: Nature and Energetics of the Ir–Ir Bonding from DFT Calculations

B. Eva Villarroya,[†] Cristina Tejel,[†] Marie-Madeleine Rohmer,*[,‡] Luis A. Oro,*[,†] Miguel A. Ciriano,[†] and Marc Bénard[‡]

Laboratoire de Chimie Quantique, UMR 7551, CNRS, and Université Louis Pasteur, Strasbourg, France, and Departamento de Química Inorgánica, Instituto Universitario de Catálisis Homogénea e Instituto de Ciencia de Materiales de Aragón, Universidad de Zaragoza-CSIC, 50009-Zaragoza, Spain

Received March 21, 2005

The structure of the Ir[I] complex $[Ir_2(\mu\text{-OPy})_2(CO)_4]$ (Opy = 2-pyridonate) has been fully characterized in its head-to-head (**A**) configuration as a "dimer of dimers" **AA** in which two binuclear complexes are connected by means of a weak, but unsupported, iridium–iridium interaction (Ir(2)···Ir(2A) 2.9808(6) Å). The head-to-tail isomer, referred to as **B**, was found in equilibrium with **A** in solution. It has been shown that this complex can be oxidized by diiodine to give iridium chains with highly selective configurations and general formula $I–[Ir_2(\mu\text{-OPy})_2(CO)_4]_n–I$ (n = 1–3). The synthesis of I**A**I **(1)**, of the isomers I**AA**I **(2AA)** and I**AB**I (2**AB**), and of I**ABA**I **(3)** is reported. DFT calculations have been carried out on **A** and **B** and on the known isomers of **1**–**3**, as well as on two isomers of the hypothetic chain of eight $Ir^{1.25}$ atoms corresponding to $n = 4$. The stability of the metal chain is assigned to a 2-electron/2n-center σ bond delocalized along the metal backbone and supplemented with a weak attractive interaction of the metallophilic type. Calculations confirm that further oxidation of the Ir chains corresponding to $n > 1$ by iodine, yielding the cleavage of one or two unsupported bond(s), is a highly exothermic process. The formation of the $I–[Ir_2(\mu\text{-OPy})_2(CO)_4]_n–I$ chains is also computed to be exothermic, either highly for $n = 1$ or still significantly for $n = 2$ and 3. At variance with these results, the formation of an octanuclear chain is predicted to be no more than marginally exothermic (ΔG = 1.7 kcal·mol^{-1}), mainly because of interligand strain induced by the steric bulk of the amidate rings.

1. Introduction

A considerable surge of interest is presently noticed in the field of chain compounds, particularly those involving transition metal backbones. In their recent highlight article on the subject, Bera and Dunbar analyze the change of perspective underlying the present renaissance of one-dimensional metal−metal chain compounds.[1] Starting in the mid-1960s from the quest for high-temperature superconductivity in 1D materials,[2] the interest has now shifted to the characterization of unusual properties typical of the quantum behavior of nanoscale molecules.[1] The characterization of versatile materials displaying structural, electric, magnetic, or photochemical bistability easily explains the current enthusiasm for these low-dimensional, oriented, and potentially conductive nanostructures that have been termed "molecular wires" or more recently "extended metal atom chains" (EMACs).[3]

Several methods have been used to stabilize EMACs. The pathway that could be termed a "ligand-driven approach" relies on the synthesis of specifically designed ligands whose number of donor sites determines the nuclearity of the complex.[1] Along these guidelines, the use of polypyridylamide ligands is generating a rapidly increasing and fascinating family of linear compounds containing from 3 to 9 metal

* To whom correspondence should be addressed. E-mail: rohmer@quantix.u-strasbourg.fr (M.-M.R.); oro@unizar.es (L.A.O.).
† Universidad de Zaragoza-CSIC.
‡ UMR 7551, CNRS, and Université Louis Pasteur.

(1) Bera, J. K.; Dunbar, K. R. *Angew. Chem., Int. Ed.* **2002**, *41*, 4453.
(2) (a) Little, W. A. *Phys. Rev. A* **1964**, *134*, 1416. (b) Coleman, L. B.; Cohen, M. J.; Sandman, D. J.; Yamagishi, F. G.; Garito, A. F.; Heeger, A. J. *Solid State Commun.* **1973**, *12*, 1125. (c) Miller, J. S., Ed. *Extended Linear Chain Compounds*; Plenum: New York, 1982; Vols. 1−3.
(3) (a) Berry, J. F.; Cotton, F. A.; Daniels, L. M.; Murillo, C. A.; Wang, X. *Inorg. Chem.* **2003**, *42*, 2418. (b) Berry, J. F.; Cotton, F. A.; Lei, P.; Lu, T.; Murillo, C. A. *Inorg. Chem.* **2003**, *42*, 3534. (c) Berry, J. F.; Cotton, F. A.; Lu, T.; Murillo, C. A. Wang, X. *Inorg. Chem.* **2003**, *42*, 3595. (d) Berry, J. F.; Cotton, F. A.; Lu, T.; Murillo, C. A. *Inorg. Chem.* **2003**, *42*, 4425. (e) Berry, J. F.; Cotton, F. A.; Murillo, C. A. *Organometallics* **2004**, *23*, 2503.

10.1021/ic050419w CCC: $30.25
Published on Web 08/23/2005

atoms.[3−5] Other types of polydentate ligands, such as unsaturated hydrocarbons, are presently investigated.[6] The other route to EMACs is a "metal-driven approach" based upon the condensation of dinuclear units bridged with lactam ligands generating mixed-valence chains with unsupported metal−metal bonds. "Platinum blues" exhibiting a linear arrangement of 4 or 8 Pt atoms still represents the most important and best studied family of such metal chains.[7] However, new chain compounds with $[Rh_4]^{6+}$, $[Ir_4]^{6+}$, and $[Ir_6]^{8+}$ metal cores were recently prepared.[8−11] It is clear from their X-ray characterization and from the first investigations carried out on their respective electronic structure[8,12] that these rhodium and iridium blues display large similarities with their platinum counterparts. However, the iridium chains, made from the assembly of two or three $[Ir_2(\mu\text{-OPy})_2(CO)_4]$ (Opy = 2-pyridonate) fragments and completed with two I^- ligands in axial position, present some fascinating specificities. It first appears (Scheme 1) that the length of the metal chain can be tuned with the molar ratio of the diiodine oxidative agent with respect to the dinuclear precursor $[(Ir^I)_2(\mu\text{-OPy})_2(CO)_4]$, present in solution as a mixture of the head-to-head (**A**) and head-to-tail (**B**) isomers:[10,11]

$$\mathbf{A} + I_2 \rightarrow I{-}[(Ir^{II})_2(\mu\text{-OPy})_2(CO)_4]{-}I \qquad \mathbf{IAI\ (1A)} \qquad (1)$$

$$\mathbf{A} + \mathbf{B} + I_2 \rightarrow I{-}[(Ir^{1.5})_2(\mu\text{-OPy})_2(CO)_4]_2{-}I \quad \mathbf{IABI\ (2AB)} \xrightarrow{\Delta} \mathbf{IAAI\ (2AA)} \qquad (2)$$

$$2\mathbf{A} + \mathbf{B} + I_2 \rightarrow I{-}[(Ir^{1.33})_2(\mu\text{-OPy})_2(CO)_4]_3{-}I \qquad \mathbf{IABAI\ (3)} \qquad (3)$$

A step by step oxidative cleavage of **2** and **3**, eventually leading to **1**, is also initiated by diiodine:

$$\mathbf{3} + I_2 \rightarrow 2\mathbf{AB} + \mathbf{1A} \quad \mathbf{2AB} + I_2 \rightarrow \mathbf{1A} + \mathbf{1B} \qquad (4)$$

An obvious question raised by eqs 1−3 concerns the possibility of extending the chain length by further restricting the diiodine supply. It should be noticed that the generation of longer chains would reduce as well the average oxidation state of iridium toward a limit of Ir^I for a hypothetic polymer of infinite length.

Scheme 1[a]

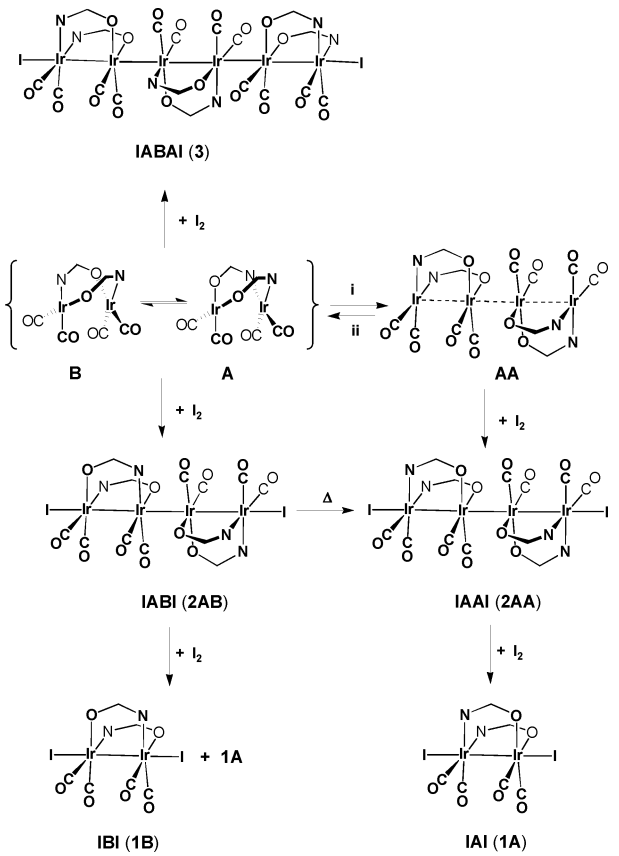

[a] Key: i = crystallization; ii = dissolution.

Another point distinguishing the platinum blues from the iridium chains concerns the selectivity of the observed structures with respect to the "head-to-head (**A**)/head-to-tail (**B**)" isomerism. These two configurations of the dinuclear building block, represented in Scheme 1, arise as a consequence of the amidate N−C−O ligand asymmetry and were found to be in a 1:1 chemical equilibrium in solution. However, the experience on platinum blues had suggested that the **AA** configuration was required for the concatenation of two dinuclear blocks,[13] since this arrangement is the only one that avoids the steric congestion originating in the presence of heterocycles across the unsupported metal−metal bond.[7] In opposition to the strict selectivity observed with platinum, the **AB** configuration of **2** was obtained in high yield at low temperature and crystallographically characterized, even though the **AA** form was shown to be thermodynamically favored. Furthermore, the trimeric assembly of **3** was characterized in the unprecedented **ABA** configuration displaying two **AB** contacts. After specifying the details of the synthetic processes, we will report the results of DFT calculations aimed at modeling the structure and the energetics of **1**−**3**, of their $Ir^I{-}Ir^I$ precursor in its dimeric form,

(4) (a) Chang, H.-C.; Li, J.-T.; Wang, C.-C.; Lin, T.-W.; Lee, H.-C.; Lee, G.-H.; Peng, S.-M. *Eur. J. Inorg.* Chem. **1999**, 1243. (b) Peng, S.-M.; Wang, C.-C.; Jang, Y.-L.; Chen, Y.-H.; Li, F.-Y.; Mou, C.-Y.; Leung, M.-K. *J. Magn. Magn. Mater.* **2000**, *209*, 80. (c) Yeh, C.-Y.; Chou, C.-H.; Pan, K.-C.; Wang, C.-C.; Lee, G.-H.; Su, Y. O.; Peng, S.-M. *J. Chem. Soc., Dalton Trans.* **2002**, 2670. (d) Tsao, T.-B.; Lee, G.-H.; Yeh, C.-Y.; Peng, S.-M. *J. Chem. Soc., Dalton Trans.* **2003**, 1465.
(5) Sheng, T.; Appelt, R.; Comte, V.; Vahrenkamp, H. *Eur. J. Inorg. Chem.* **2003**, 3731.
(6) (a) Murahashi, T.; Kurosawa, H. *Coord. Chem. Rev.* **2002**, *231*, 207. (b) Tatsumi, Y.; Naga, R.; Nakashima, H.; Murahashi, T.; Kurosawa, H. *Chem. Comm.* **2004**, 1430.
(7) Matsumoto, K.; Sakai, K.; Nishio, K.; Tokisue, Y.; Ito, R.; Nishide, T.; Shichi, Y. *J. Am. Chem. Soc.* **1992**, *114*, 8110 and references therein.
(8) Tejel, C.; Ciriano, M. A.; López, J. A.; Lahoz, F. J.; Oro, L. A. *Angew. Chem., Int. Ed.* **1998**, *37*, 1542.
(9) Tejel, C.; Ciriano, M. A.; Oro, L. A. *Chem.*—Eur. J. **1999**, *5*, 1131.
(10) Tejel, C.; Ciriano, M. A.; Villarroya, B. E.; Gelpi, R.; López, J. A.; Lahoz, F. J.; Oro, L. A. *Angew. Chem., Int. Ed.* **2001**, *40*, 4084.
(11) Tejel, C.; Ciriano, M. A.; Villarroya, B. E.; López, J. A.; Lahoz, F. J.; Oro, L. A. *Angew. Chem., Int. Ed.* **2003**, *42*, 530.
(12) O'Halloran, T. V.; Mascharak, P. K.; Williams, I. D.; Roberts, M. M.; Lippard, S. J. *Inorg. Chem.* **1987**, *26*, 1261.
(13) (a) Matsumoto, K.; Sakai, K. *Adv. Inorg. Chem.* **2000**, *49*, 375. (b) Lippert, *Coord. Chem. Rev.* **1999**, *182*, 263. (c) Sakai, K.; Tanaka, Y.; Tsuchiya, Y.; Hirata, K.; Tsubomura, T.; Iijima, S.; Bhattacharjee, A. *J. Am. Chem. Soc.* **1998**, *120*, 8366.

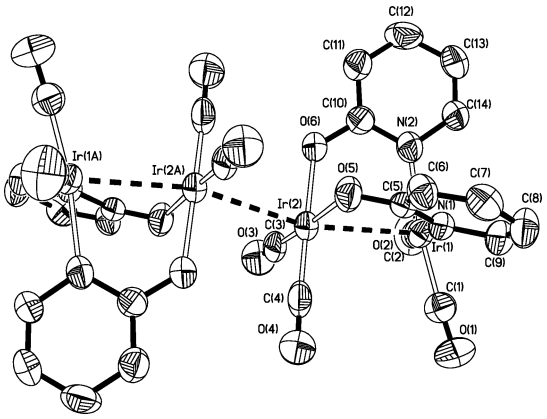

Figure 1. Molecular structure and atomic labeling of the complex $[Ir_2(\mu\text{-Opy})_2(CO)_4]$ showing the "dimer of dimers" **AA** found in the unit cell. Ellipsoids are drawn at the 50% probability level. Hydrogen atoms are omitted for clarity.

and of the hypothetic octanuclear chain $I-[(Ir^{1.25})_2(\mu\text{-OPy})_2(CO)_4]_4-I$ (**4**). The σ-delocalized nature of the bonding along the metal chain will be confirmed and a thermodynamic model of reactions 1−4 proposed. The effect of oxidation on the structure of **2** will be discussed and extended to **3** in relation with the sequence of the metal σ orbitals. Finally, the problem of **AB** vs **AA** isomerism will be examined in **2** and considered in relation to the feasibility of longer iridium chains.

2. Results and Discussion

2.1. Syntheses. The precursor for the iridium pyridonate chains was the dinuclear complex $[Ir_2(\mu\text{-Opy})_2(CO)_4]$ (Opy = 2-pyridonate), which was isolated as air-sensitive copper-like crystals with metallic luster by bubbling carbon monoxide slowly through a carefully deoxygenated solution of the complex $[Ir_2(\mu\text{-Opy})_2(cod)_2]$ in toluene.[14] The X-ray structure of $[Ir_2(\mu\text{-Opy})_2(CO)_4]$ revealed the complex to be the head-to-head isomer (**A**) forming the dimer **AA** shown in Figure 1.

Each binuclear complex possesses a HH, or **A**-configuration, for the bridging ligands, which hold the metals in close proximity (Ir(1)···Ir(2) 2.8693(5) Å), generating two different types of iridium centers, O,O- and N,N-coordinated. In addition, two dinuclear units form a dimer (**AA**) through an intermolecular iridium−iridium interaction (Ir(2)···Ir(2A) 2.9808(6) Å) that occurs between the O,O-coordinated iridium atoms, i.e., between the less hindered faces.

While $[Ir_2(\mu\text{-Opy})_2(cod)_2]$ was found to be the pure HT, or **B** isomer (C_2), in solution, its carbonylation provides a solution of $[Ir_2(\mu\text{-Opy})_2(CO)_4]$ containing the **A** and **B** isomers, from which the pure **A** isomer crystallizes as the **AA** dimer. Conversely, this solid dissolves slowly in benzene or toluene on heating to give a 1:1 mixture of the **A** (C_s) and **B** (C_2) isomers, as determined by ^{1}H NMR spectroscopy. Both show four signals for the equivalent 2-pyridonate ligands in the ^{1}H NMR spectrum according to their symmetry. As expected, these configurational isomers were found to be in a chemical equilibrium, as shown by the ^{1}H two-dimensional exchange (EXSY) spectrum (Figure 2). Moreover, the 1:1 ratio of the isomers in equilibrium was found unaltered when the spectrum was recorded at 65 °C, which indicates the free energy exchange for the equilibrium to be close to zero. ($\Delta G \approx 0$; $\Delta G = -RT \ln K$). However, the limited solubility of the **AA** dimer shifts the equilibrium to the **A** isomer, as it crystallizes out.

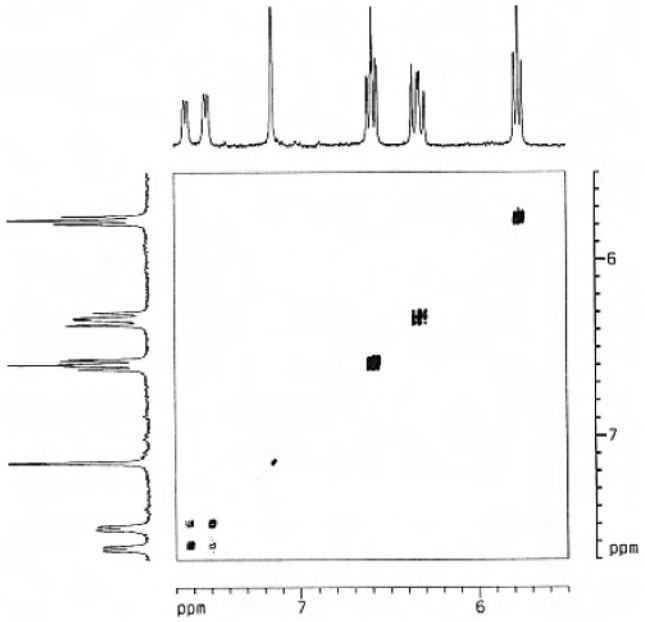

Figure 2. ^{1}H two-dimensional exchange (EXSY) spectrum of the complex $[Ir_2(\mu\text{-Opy})_2(CO)_4]$ in C_6D_6 showing the cross-peaks between the head-to-head **A** and the head-to-tail **B** isomers (mixing time 500 ms). The singlet at δ 7.15 ppm corresponds to the residual signal of the solvent.

The **A** → **B** isomerization that occurs on dissolving **AA** was found to be slower than the reactions of a mixture of **A** and **B** with iodine, thus providing a way to control whether the reactive isomer is the pure **A** form or the equimolecular mixture of **A** and **B**. Therefore, addition of solid $[Ir_2(\mu\text{-Opy})_2(CO)_4]$ (**AA**) to a toluene solution of diiodine (in 1:0.5 molar ratio) gave the isomer I**AA**I pure, while the pure isomer I**AB**I resulted if the reaction was carried out with a solution of $[Ir_2(\mu\text{-Opy})_2(CO)_4]$, which contains an equimolar mixture of **A** and **B** in equilibrium, in toluene at 0 °C. The X-ray crystal structures of I**AA**I and I**AB**I have been reported in a previous communication.[10]

The stability found in solution for these diamagnetic tetrairidium chains is remarkable, remaining as such in solution, which allows the spectral characterization by NMR spectroscopy. The equivalence of the four 2-pyridonate ligands observed in the ^{1}H NMR spectrum of the complex I**AA**I is indicative of an averaged C_{2h} symmetry for the molecule in solution, which can be achieved by a slight rotation of the dinuclear moieties around the unsupported metal−metal bond. However, the 2-pyridonate ligands are nonequivalent in complex I**AB**I, since this compound has no symmetry element (C_1 chiral).

On the other hand, a solution of the green complex I**AB**I was found to evolve into the blue isomer I**AA**I on heating

(14) (a) Ciriano, M. A.; Villarroya, B. E.; Oro, L. A.; Foces-Foces, C.; Cano, F. H. *J. Organomet Chem.* **1989**, *266*, 277. (b) Rodman, G. S.; Mann, K. R. *Inorg. Chem.* **1988**, *27*, 3338.

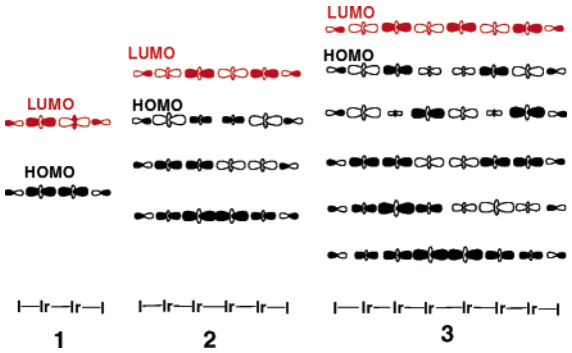

Figure 3. Representation of the σ delocalized frontier orbitals of complexes **1**−**3**.

at 60 °C in less than 5 min. This transformation, quantitative by ^{1}H NMR spectroscopy, occurred also at room temperature but more slowly. Indeed, the preparation and isolation of I**AB**I was achieved at low temperature, to avoid the isomerization of I**AB**I into I**AA**I, starting from a solution containing **A** and **B**. From these experiments, it is now clear that complex I**AA**I is the thermodynamic product while complex I**AB**I corresponds to the kinetic product from the reaction of the mixture of **A** and **B**, in equilibrium, with diiodine.

The experimental characterization of an **AB** configuration in tetrametallic chains suggests that hexanuclear chains in which two **A** units sandwich a **B** complex should be feasible. Effectively, the oligomer I**ABA**I resulted from the addition of solid diiodine to a solution of **A** and **B** in toluene at 0 °C (in 1:3 molar ratio). The previously reported[11] molecular structure of I**ABA**I showed the six iridium atoms linked by metal−metal bonds, two of which are unsupported by bridging ligands. The hexametallic chain was found to be thermally stable in the solid state and under 0 °C in solution. Moreover, the C_2 symmetry of the species in solution, which is accessible by a slight rotation of the three dinuclear moieties around the unsupported iridium−iridium bonds, is evidenced by the observation of three inequivalent α-pyridonate bridging ligands in the ^{1}H NMR spectrum.

The hexametallic chain in complex I**ABA**I can be broken step by step maintaining the configuration of the individual links. Thus, the addition of diiodine to I**ABA**I produced I**AB**I along with the diiridium(II) complex I**A**I. A further reaction of I**AB**I with diiodine gave an equimolar mixture of I**A**I and its configurational isomer I**B**I. The HH and HT configurations were established from the X-ray crystal structure determination of complex I**A**I [11] and the ^{1}H NMR spectrum of this mixture.

2.2. Structural Effects of a Delocalized σ Bond. Delocalized σ Bonding along the Chain. The question of the bonding along iridium chains has been addressed by means of extended Hückel (EH) MO calculation in a previous work focused on the tetranuclear complex **2**.[11] A qualitative fragment MO diagram represents the sequence of four MOs made from all possible combinations of the metal d_{z^2} orbitals (Figure 3). The energy of these MOs increases with the number of nodes along the chain. All levels are doubly occupied, except the highest one, which develops an antibonding character between every pair of adjacent metal atoms. The vacancy of this high-energy σ MO is therefore responsible for the unsupported bond between the two pyridonate-bridged moieties. In a more general way, it provides the whole iridium chain with a fully delocalized σ bonding (2-electron/4-center bond), as a mirror image of the delocalized and *fully* antibonding character of the empty MO. It also supports an equal distribution along the metal backbone of the 6+ formal charge, resulting in a fractional oxidation state of +1.5 for each metal center.

Let us now complete this interpretation of the metal−metal bonding in **2** with the similar EHMO orbital diagrams obtained for the dinuclear complex **1** and for the hexanuclear chain **3** (Figure 3). The diagram for **1** displays the classical sequence of frontier MOs associated with a metal−metal single σ bond. The diagram for **3** represents a plain extension of the diagram for **2**, with all six σ MOs doubly occupied, except the highest one, which remains vacant. This yields a delocalized 2-electron/6-center σ bond. It is now easy to generalize this bonding scheme to any hypothetic iridium wire composed of n dimeric units on the model of **1**−**3**: I−[$Ir_2(\mu$-OPy$)_2$(CO)$_4$]$_n$−I. The formal positive charge of the metal backbone is $2n + 2$, which corresponds to a total of $16n - 2$ metal electrons. All MOs belonging to the t_{2g} set are doubly occupied, so that $4n - 2$ electrons are to be accommodated on the σ MOs according to the aufbau principle. Should it be $4n$ that *all* σ MOs would be filled, the chain would either break apart or at least experience an important stretching of the Ir−Ir distances as in the **AA** dimer due to the vanishing of the delocalized bond. In all iridium chains of this type, real or hypothetic, the delocalized bonding which firmly holds the dimeric units together originates in the 2-electron oxidation of the complex by diiodine.

Another source of metal−metal bonding should be expected from the 5d → 6sp density transfer, a mutual donation/back-donation process which is at least partly responsible for the so-called metallophilic interaction between metal atoms in a closed-shell electronic configuration.[15] This density transfer is active along the z axis and should increase with the population of the d_{z^2} donor orbitals. This population is maximal in the Ir(I) precursors. In the oxidized species, the population of individual d_{z^2} iridium orbitals is increasing with the size of the metal chain, as a consequence of the proportion of σ MOs being doubly occupied and of the correlated decrease of the metals oxidation state. Metallophilic interactions are therefore expected to partly counterbalance the expected decline of the delocalized 2-electron/2n-center bond strength as n increases.

Every metal σ MO displays an antibonding character with respect to the terminal iodines (Figure 3). These d_{z^2}/p_z interactions correspond to the out-of-phase counterpart of the σ-donation process from the terminal ligands to the Ir chain. Consequently, the overall strength of the Ir−I bonds tends to be reduced as the proportion of these occupied σ

(15) (a) Scherbaum, F.; Grohmann, A.; Huber, B.; Krüger, C.; Schmidbaur, H. *Angew. Chem., Int. Ed. Engl.* **1988**, *27*, 1544. (b) Pyykkö, P.; Li, J.; Runeberg, N. *Chem. Phys. Lett.* **1994**, *218*, 133. (c) For a recent review, see: Pyykkö, P. *Angew. Chem., Int. Ed.* **2004**, *43*, 4412.

Table 1. Selected Bond Lengths (Å) Observed and Computed in the I−[$Ir_2(\mu$-OPy)$_2$(CO)$_4$]$_n$−I Complexes (n = 1−4)[a]

				I**AA**I		I**AB**I			I**ABA**I		
	I**A**I obsd	I**A**I comp	I**B**I comp	obsd	comp	obsd	comp	[I**AB**I]$^+$ comp	obsd	comp	I**ABBA**I comp
Ir(1)−Ir(2)	2.639	2.722	2.723	2.701	2.772	2.692[b]	2.781[b]	2.766[b]	2.700	2.799	2.800
Ir(2)−I r(3)				2.750	2.827	2.779	2.886	2.946	2.787	2.911	2.920
Ir(3)−I r(4)						2.711	2.767	2.772	2.697	2.799	2.820
Ir(4)−I r(5)											3.080
Ir_{NN}−I	2.784	2.924		2.843	2.982	2.847	2.977	2.886	2.853	2.999	3.002
Ir_{OO}−I	2.740	2.826									
Ir_{NO}−I			2.871			2.821	2.904	2.836			
Ir−O(S)	2.042	2.070	2.066	2.007	2.078	2.045	2.067	2.059	1.994	2.082	2.079
Ir−O(L)	2.060	2.072	2.066	2.035	2.083	2.087	2.085	2.068	2.084	2.091	2.094
Ir−N(S)	2.098	2.124	2.124	2.113	2.129	2.120	2.126	2.114	2.08(2)	2.129	2.130
Ir−N(L)	2.112	2.130	2.124	2.14	2.135	2.132	2.134	2.133	2.13(2)	2.135	2.143
Ir−C(S)	1.856	1.880	1.879	1.84	1.870	1.81	1.869	1.877	1.73(3)	1.865	1.860
Ir−C(L)	1.903	1.900	1.901	1.91	1.893	1.885	1.894	1.907	1.93(3)	1.891	1.890

[a] The range of the Ir−X distances (X = O, N, C) is given with the largest (L) and the smallest (S) of these distances. For symmetric chains, only nonequivalent Ir−Ir bond lengths are reported. [b] **A** side.

combinations increases with n. An elongation of the Ir−I bonds is therefore expected as the metal chain extends.

Observed and Computed Structures of the Oxidized Ir Chains. Selected interatomic distances taken from the geometries optimized for the known isomers of **1** (I**A**I and I**B**I), **2** (I**AA**I and I**AB**I), and **3** (I**ABA**I) are displayed in Table 1, together with the corresponding distances reported from the observed structures, when available. The distances calculated for the oxidized form of I**AB**I, [I**AB**I]$^+$, and for the still hypothetic tetramer I**ABBA**I are also reported.

The distances between the metal and its equatorial ligands are not significantly affected by the length of the complex. The difference between the shortest and the longest distance of the same type is always smaller than 0.03 Å. The large range of distances sometimes noted in the observed structures (up to 0.07 Å for Ir−O and to 0.20 Å for Ir−C in **3**) should probably be assigned to a relatively large standard deviation. Despite the overestimation of the computed Ir−Ir and Ir−I distances, most observed structural trends are well reproduced and sometimes amplified by the calculations. The unsupported metal−metal bonds are computed longer than the bridged ones, by 0.055 Å for the **AA** contacts (observed: 0.05 Å) and by 0.10−0.12 Å for the **AB** contacts (observed: 0.07−0.09 Å). The sensitivity of the unsupported Ir−Ir bond lengths to the conformational arrangement of the equatorial ligands is further illustrated by the Ir_B−Ir_B bond in I**ABBA**I (3.08 Å) being again 0.16 Å longer than the Ir_B−Ir_A contact in the same compound (Table 1). The length of the *bridged* Ir−Ir bond increases by 0.05 Å from **1** to **2**, and this terminal bond tends to stretch more in the higher polymers but at a much slower pace (Δ(Ir−Ir)$_{term.}$ = 0.028 Å from I**AA**I to I**ABBA**I). A similar difference (0.034 Å) is computed for the unsupported Ir_A−Ir_B bond length between I**AB**I and I**ABBA**I. Depending on various factors such as the strength of the bonding interaction, which decreases with the system size, the supported or unsupported nature of the bond, and the ligand−ligand steric contacts, the computed Ir−Ir bond lengths extend over a very broad range of 0.36 Å, from 2.722 Å in I**A**I to 3.08 Å for the central bond of the hypothetic tetramer. In a single compound such as I**ABBA**I, the range of the metal−metal distances extends over 0.28 Å.

The Ir−I bond lengths also appear highly sensitive to the nature of the equatorial ligand ends. The Ir_{NN}−I and the Ir_{OO}−I in I**A**I differ by 0.10 Å (observed difference: 0.044 Å), the Ir_{NO}−I distances in I**B**I being almost exactly average (Table 1). This could be assigned to intramolecular interactions between iodine and pyridonate hydrogens. Two such nonbonded contacts, with I···H comprised between 2.75 and 2.85 Å, are obtained in the optimized geometries of each isomer. In the C_s I**A**I isomer, both contacts occur on the NN side, which corresponds to the longest Ir−I bond. In the C_2 I**B**I complex, the contacts are shared between the two molecular ends. The computed Ir−I distances of any type also stretch with the size of the complex, due to the increasing number of occupied σ-type MOs with antibonding Ir−I character (Figure 3). This trend is confirmed by the X-ray structures for the Ir_{NN}−I bonds (Table 1).

Special attention should be paid to the computed structure of the oxidized tetranuclear chain, [I**AB**I]$^+$. According to the bonding scheme summarized in Figure 3, oxidation results in the removal of one electron from the σ-delocalized HOMO. As all σ-type orbitals, the HOMO is antibonding between the terminal Ir atoms and iodine. As expected, both Ir−I bond lengths decrease upon oxidation, but the magnitude of this contraction (0.068 Å for Ir_{NO}−I; 0.091 Å for Ir_{NN}−I) may appear surprising. These computed changes are however in good agreement with the contraction of the Cu−Cl bond length *observed* when the linear chain of metal atoms Cu_3(dipyridylamide)$_4Cl_2$ is oxidized (0.071 Å < Δd < 0.099 Å depending upon crystal environment and temperature).[3a,16] In the present case, ∼50% of the weight of the HOMO/SOMO is concentrated on the terminal Ir atoms, which hence carry out half of the extra charge (Figure 3). One could therefore argue that the bond length contraction has been amplified by the electrostatic attraction between these terminal metal atoms and the negatively charged iodines. The central, unsupported Ir−Ir bond is elongated by 0.06 Å, in agreement with the bonding character of the HOMO between Ir2 and Ir3 (Figure 3). Since the same orbital is clearly antibonding between the pyridonate-bridged metals, one could expect a contraction of the Ir1−Ir2 and of the Ir3−

(16) Berry, J. F.; Cotton, F. A.; Lei, P.; Murillo, C. A. *Inorg. Chem.* **2003**, *42*, 377.

Ir4 distances with respect to the neutral complex, but the equilibrium geometry shows no clear trend (Table 1). The bond contraction induced by the partial depopulation of an antibonding MO is almost completely offset by the increased repulsion stemming from the positively charged metal atoms. An analysis of the HOMO in **3** suggests that a one-electron oxidation of this complex should result in an elongation of the central (now supported) Ir−Ir bond, little change in the other metal−metal bonds, and a contraction of the Ir−I distances somewhat smaller than for **2**.

Structure and Bond Strength of the Precursor Dimer AA. The crystal structure of the precursor consists of dimeric **AA** entities in which the monomers are connected by an unsupported Ir−Ir contact of ∼2.98 Å (Figure 1). The two metals in each monomer are also at a bonding distance of ∼2.87 Å. The structure of the metal chain in **AA** therefore resembles that of I**AA**I, except that the central and the terminal Ir−Ir bond lengths have been stretched by 0.23 and 0.17 Å, respectively. Since the metal is Ir(I), this weak metal−metal interaction cannot be assigned to any covalent σ bonding and should be attributed to metallophilic attraction.[15] The same type of interaction should explain the structure of polymeric chains of nonbridged ruthenium or osmium atoms having the general formula $[M^0(\text{bipyridine})(CO)(L)]_n$ (L = CO, CH_3CN).[17] It is well-known that the dispersion forces that account for most of the metallophilic attraction are poorly accounted for by most exchange-correlation functionals and, especially, by B3LYP and other hybrid functionals.[15c] It has been suggested however that GGA functionals and, more specifically, PW91 could provide in some cases an acceptable description of dispersion effects.[18] Indeed, calculations carried out with the B3LYP functional yield Ir−Ir distances that are far too long (3.14 and 3.03 Å). At variance with this result, calculations carried out with Slater TZP basis sets on the atomic valence shells and the BP86 functional confirm the existence of a weak Ir−Ir bonding along the chain of metal atoms with computed distances of 3.075 Å for the central bond and 2.906 Å for the terminal ones. The PW91 functional provides quite similar results (3.066 and 2.901 Å). The bond energy between the two monomers was calculated to be 6.6 kcal·mol^{-1}.

2.3. Thermodynamics of the Formation and Oxidative Cleavage of the Ir Chains. Oxidative Cleavage. Calculations confirm that all the stages of the diiodine-induced oxidative cleavage of the iridium chain polymers according to eq 4 are largely exothermic (Figure 4). It also appears that the cleavage of the unsupported Ir−Ir bonds is easier in the "long" chains of complexes **4** and **3** than in both isomers of **2**. This trend is in keeping with the mitigation of the delocalized bond strength as the number of Ir centers increases and with the rise of the steric strain in the long chains.

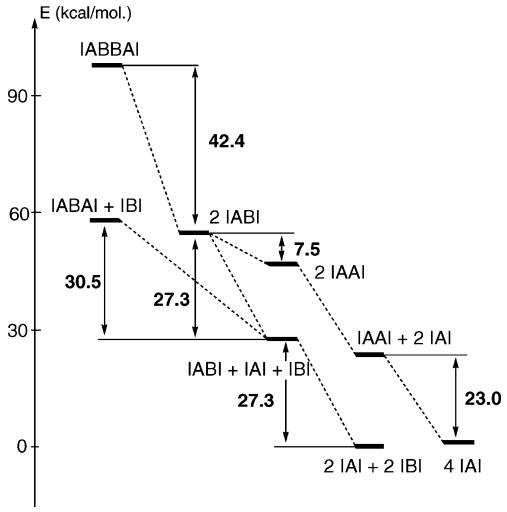

Figure 4. Computed enthalpies (kcal·mol^{-1}) associated with the stepwise oxidative cleavage of **4** and **3** by diiodine.

Starting from the hypothetic tetramer I**ABBA**I, the breaking of the weak central bond (3.08 Å, Table 1) and the addition of 1 equiv iodine yield two molecules of I**AB**I. The reaction is computed to be exothermic by 42.4 kcal·mol^{-1}. Starting now from I**ABA**I, the oxidative cleavage by iodine of one unsupported bond also leading to I**AB**I is exothermic by only 30.5 kcal·mol^{-1} (Figure 4). It has been shown that I**AB**I can be thermally converted into the more stable isomer I**AA**I. The energy difference between the two isomers is calculated to be 3.75 kcal·mol^{-1}. Both isomers of **2** can be eventually converted by reaction with diiodine either into **IAI** + **IBI**, with an exothermicity of 27.3 kcal·mol^{-1}, or into two molecules of I**A**I, then releasing 23.0 kcal·mol^{-1} (Figure 4). Both isomers of **1** are computed to be almost isoenergetic**,** with a difference of only 0.5 kcal·mol^{-1} in favor of I**B**I.

Formation. The formation process of the iridium chains from their elementary components is formally described by eqs 1−3. These equations can be seen as involving two distinct processes: (i) the oxidative addition of 1 equiv of diiodine to the **A** or **B** form of the precursor, leading to I**A**I or I**B**I, respectively, and (ii) if the final chain contains more than one dimetal unit, the insertion of one or several molecule(s) of precursor into the oxidized system. Calculations show that the energetic balance of the oxidation process is largely exothermic and little affected by the conformation of the precursor.

The energy yields associated with the formation of I**A**I and I**B**I are calculated to be 39.8 and 39.5 kcal·mol^{-1}, respectively. Both oxidized conformers are isoenergetic to within 0.5 kcal·mol^{-1}. Then, the first step of the metal chain growth is formally described by the following equations, both leading to the reaction product characterized as I**AB**I:

$$\mathbf{A} + \text{I}\mathbf{B}\text{I} \rightarrow \text{I}\mathbf{AB}\text{I} \quad (5)$$

$$\mathbf{B} + \text{I}\mathbf{A}\text{I} \rightarrow \text{I}\mathbf{AB}\text{I} \quad (6)$$

In a subsequent step, the concatenation of one more molecule of precursor yields the six-iridium chain characterized as I**ABA**I. A further insertion step formalizes the

(17) (a) Masciocchi, N.; Sironi, A.; Chardon-Noblat, S.; Deronzier, A. *Organometallics* **2002**, *21*, 4009. (b) Hartl, F.; Mahabiersing, T.; Chardon-Noblat, S.; Da Costa, P.; Deronzier, A. *Inorg. Chem.* **2004**, *43*, 7250.

(18) (a) Wesolowski, T. A.; Parisel, O.; Ellinger, Y.; Weber, J. *J. Phys. Chem.* **1997**, *101*, 7818. (b) Lorenzo, S.; Lewis, G. R.; Dance, I. *New J. Chem.* **2000**, *24*, 295.

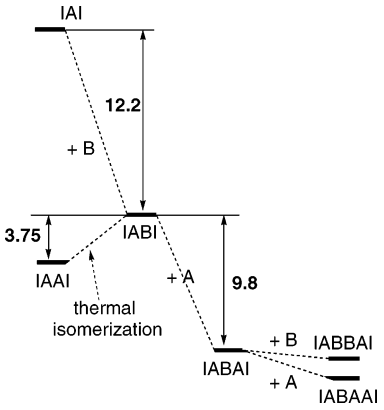

Figure 5. Computed enthalpies (kcal·mol^{-1}) of formation and isomerization of the iridium chain compounds I−[Ir$_2$(μ-OPy)$_2$(CO)$_4$]$_n$−I (n = 2−4), from the oxidized dinuclear complex I**A**I.

synthesis of a still hypothetic eight-metal chain such as I**ABBA**I or I**ABAA**I. The characterization of any of these metal chains requires the corresponding insertion process to be exothermic. Figure 5 displays the calculated enthalpy changes associated with subsequent insertion steps, starting from I**A**I. A more comprehensive diagram is available as Supporting Information (Figure S1).

The formation of I**AB**I via process (5) or (6) is calculated to be exothermic by 12.5 or 12.2 kcal·mol^{-1}, respectively. Thermal isomerization of I**AB**I yields I**AA**I as the most stable isomer with an energy difference of 3.75 kcal·mol^{-1} and a 0.06 Å contraction calculated for the unsupported Ir−Ir bond (observed contraction: 0.03 Å) (Table 1). The successful synthesis and characterization of I**ABA**I through reaction 3 at 0 °C also suggests that the obtained isomer of **3** should be thermodynamically favored with respect to I**AB**I and **A**. The hexairidium chain was indeed found more stable than the two fragments by 9.8 kcal·mol^{-1} (Figure 5).

Could the process of constructing longer metal chains be continued by further restricting the iodine supply? Calculations were expected to predict the feasibility of the octanuclear chain complex **4** by comparing the relative stability of **4** to that of the most stable parent compound, **3**, in the I**ABA**I form. Problems arise, however, since the configurational preference of complex **4** is not known and will require in any case unprecedented contacts between subsequent pyridonate-bridged dimeric units. The configuration that seems a priori most probable is the I**ABBA**I form, which is the only one that avoids two bulky pyridonate rings to lie side by side in the core of the complex, as in the projection of Figure 7. This configuration involves an unprecedented **BB** contact. Since the **B** fragment is chiral, this contact generates three isomers depending on the relative arrangement of the nitrogen and oxygen ends on Ir4 and Ir5 in I**ABBA**I; two of them are enantiomers, and the third isomer is the *meso* form. The upper part of Figure 6 shows the three isomers for the hypothetical complex I**BB**I, which models the central core of the octanuclear I**ABBA**I complex.

The lower part of Figure 6 displays the relative energies computed for the three less hindered conformations of the possible isomers of I**BB**I with respect to the conformation of lowest energy, I**AA**I. It confirms that the **BB** contact

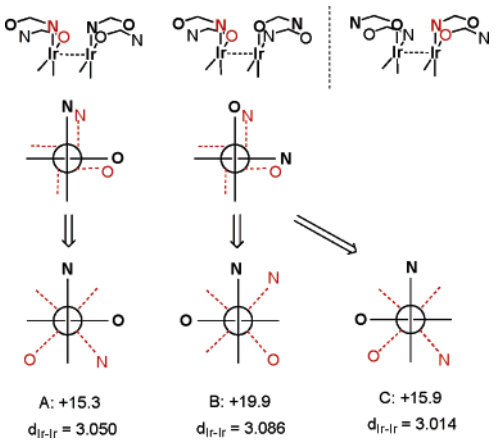

Figure 6. Three isomers of the hypothetic complex I**BB**I. Shown are central Ir2−Ir3 distances (Å) and relative energies with respect to I**AA**I (kcal·mol^{-1}) calculated for the three less constrained conformations of the equatorial ligands around the Ir2−Ir3 bond.

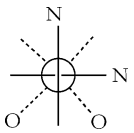

Figure 7. Conformation around the unsupported bond of the **AA** sequence in I**AABA**I showing the strained **AA** contact.

induces a penalty which is much larger than for **AB** (3.75 kcal·mol^{-1}). This result is in keeping with the very large value of 3.08 Å optimized for the central Ir−Ir bond of **4** while assuming the most favorable conformation for the **BB** contact (Figure 6).

Despite the steric strain associated with the **BB** contact, the thermodynamic balance of I**ABBA**I does not definitely rule out the possibility of obtaining an octanuclear chain complex. Indeed, the enthalpy associated with eq 7 is computed to be very close to zero (−0.2 kcal·mol^{-1}).

$$\mathbf{B} + \text{I}\mathbf{ABA}\text{I} \rightarrow \text{I}\mathbf{ABBA}\text{I} \qquad (7)$$

The possibility for the lowest isomer of **4** to correspond to a different arrangement of the four pyridonate-bridged units could not be excluded, however. A possible competitor to the I**ABBA**I isomer is the I**AABA**I skeleton, which supposedly displays a strained contact between the two subsequent **A** fragments (Figure 7)

Indeed, isomer I**AABA**I was computed to be marginally more stable than I**ABBA**I, by 1.5 kcal·mol^{-1}. As could be predicted, the weak link in this isomer is the strained **AA** contact, with a computed Ir−Ir distance of 3.070 Å. The other metal−metal distances are ∼2.925 Å if unsupported and comprised between 2.808 and 2.815 Å when supported. The thermodynamic balance for this compound however remains very tight, and a successful characterization has remained elusive up to now.

3. Summary and Conclusions

Oxidation of a [(Ir^{I})$_2$(μ-Opy)$_2$(CO)$_4$] precursor with iodine results in the condensation of n molecules of the precursor into a complex with formula I−[Ir$_2$(μ-OPy)$_2$(CO)$_4$]$_n$−I displaying a linear chain of 2n Ir atoms. The value of n,

presently limited to 3, is conditioned by the stoichiometry of the iodine supply. The transfer of one electron pair from the metal backbone to the terminal iodine ligands depopulates the e_g metal level with highest energy, which happens to be the σ-type orbital with $n - 1$ nodes between metal atoms, for all values of n. As a mirror image of this LUMO, the set of $n - 1$ doubly occupied σ orbitals globally displays a bonding character, fully delocalized along the metal framework. The strength of this delocalized 2-electron/2n-center bond obviously dilutes among the pairs of metal atoms as the fractional oxidation state of iridium, equal to $1 + 1/n$, comes closer to 1. A straightforward consequence of this bond weakening is the immediate breaking of the chains corresponding to $n = 2$ or 3 into smaller oxidized pieces by reaction with diiodine. In this family of iridium complexes, oxidation state 1, corresponding to a full occupancy of the set of metal σ MOs should be realized in two limiting cases: (i) the $[(Ir^I)_2(\mu\text{-OPy})_2(CO)_4]$ precursor; (ii) a linear chain with infinite length. Such an infinite chain has not been synthesized with iridium amidates, but 1D polymers have been characterized with isoelectronic Ru^0 and Os^0.[17] The $[(Ir^I)_2(\mu\text{-OPy})_2(CO)_4]$ precursor has been reported in the present work to have a dimeric structure. Both clues suggest that a weak, noncovalent bonding of the metallophilic type does account for the unsupported bonds between d^8 metals and is probably superimposed to the stronger covalent bonding in the oxidized iridium chains.

Could the concatenation of diiridium precursors be extended beyond $n = 3$? As discussed already for platinum blues, the use of amidate bridging ligands generates steric hindrance when the heterocyclic side of the ligand is facing another dimetallic entity across an unsupported M−M bond. Indeed, complex **3** represents the first metal−pyridonate chain in which such a ligand arrangement could be observed, through the I**ABA**I conformation. Calculations show that the exothermic balance of the oxidation of the diiridium precursor sharply decreases from 40 kcal·mol^{-1} to 12.5 and 9.8 kcal·mol^{-1} as soon as concatenation occurs with $n = 2$ and 3, respectively. The assembly of four precursor units would require an unsupported Ir−Ir bond with still more intense strain resulting from the sequence of two units either both in the **B** configuration or in the **A** configuration with two heterocycles facing the bond. The I**ABAA**I configuration seems to be the best candidate for an octanuclear chain of iridium atoms, but its predicted exothermicity of only 1.7 kcal·mol^{-1} with respect to I**ABA**I + **A** makes its synthesis and characterization a really difficult challenge.

4. Experimental and Computational Section

Starting Materials and Physical Methods. All reactions were carried out under argon using standard Schlenk techniques. The compound $[Ir_2(\mu\text{-OPy})_2(cod)_2]$ was prepared according to literature methods.[14] Solvents were dried and distilled under argon before use by standard methods. Carbon, hydrogen, and nitrogen analyses were performed with a Perkin-Elmer 2400 microanalyzer. IR spectra were recorded with a Nicolet 550 spectrophotometer. ^{1}H and ^{13}C-{^{1}H} NMR spectra were recorded on Bruker ARX 300 and on Varian UNITY 300 spectrometers operating at 300.13 and 299.95 MHz for ^{1}H, respectively. Chemical shifts are reported in parts per million and referenced to $SiMe_4$ using the residual signal of the deuterated solvent as reference.

Synthesis of the Complexes. $[Ir_2(\mu\text{-OPy})_2(CO)_4]$. Carbon monoxide was bubbled for 45 min through a solution of $[Ir_2(\mu\text{-OPy})_2(cod)_2]$.(500 mg, 0.63 mmol) in toluene (10 mL). The initial red solution turns purple, and $[Ir_2(\mu\text{-OPy})_2(CO)_4]$ crystallized out spontaneously from the solution as needles with a copper-like appearance suitable for X-ray diffraction. The solution was decanted, and the crystals were washed with hexane (3 × 5 mL) and vacuum-dried. Yield: 350 mg (81%). Anal. Calcd for $C_{14}H_8N_2O_6Ir_2$: C, 24.56; H, 1.18; N, 4.09. Found: C, 24.95; H, 1.47; N, 4.18. IR (toluene): ν(CO) = 2079 (s), 2048 (m), 2002 (s) cm^{-1}. ^{1}H NMR (C_6D_6, 60 °C): **A** isomer, δ = 7.64 (d, 6.9 Hz, 2H), 6.60 (ddd, 8.7, 6.9, 1.8 Hz, 2H), 6.36 (d, 8.7 Hz, 2H), 5.77 (t, 6.9 Hz, 2H); **B** isomer, δ = 7.53 (d, 6.9 Hz, 2H), 6.60 (ddd, 8.7, 6.9, 1.8 Hz, 2H), 6.31 (d, 8.7 Hz, 2H), 5.77 (t, 6.9 Hz, 2H).

$[Ir_6(\mu\text{-OPy})_6(I)_2(CO)_{12}]$ (IABAI, 3). Addition of solid diiodine (7.6 mg, 0.030 mmol) to a toluene solution of $[Ir_2(\mu\text{-OPy})_2(CO)_4]$ (61.6 mg, 0.090 mmol) at 0 °C gave immediately a dark-blue solution. This solution was carefully layered with hexane and maintained at −30° for 3 days to render a crystalline solid having a copper-like appearance. The solution was decanted, and the crystals were washed with hexane and vacuum-dried. Yield: 53 mg (75%). Anal. Calcd for $C_{42}H_{24}N_6O_{18}I_2Ir_6\cdot 0.5C_6H_{14}$: C, 22.99; H, 1.33; N, 3.57. Found: C, 23.12: H, 1.39; N, 3.49. IR (Nujol): ν(CO) = 2101 (sh), 2079 (s), 2061 (sh), 2042 (s), 2023 (sh), 2007 (sh) cm^{-1}. ^{1}H NMR ([D$_8$]toluene, −50 °C): δ = 9.74 (dd, 6.3, 1.8 Hz, 2H), 9.68 (d, 6.3 Hz, 2H), 9.56 (dd, 6.3, 1.8 Hz, 2H), 6.58 (td, 8.4, 2.1 Hz, 2H), 6.49 (m, 4H), 6.35 (td, 7.2, 1.5 Hz, 2H), 6.17 (d, 8.4 Hz, 2H), 6.10 (d, 8.1 Hz, 2H), 5.98 (td, 7.2, 1.3 Hz, 2H), 5.69 (m, 4H).

$[Ir_4(\mu\text{-OPy})_4(I)_2(CO)_8]$ (I**AB**I, **2AB)** was prepared as described above for I**ABA**I starting from $[Ir_2(\mu\text{-OPy})_2(CO)_4]$ (68.5 mg, 0.10 mmol) and diodine (12.7 mg, 0.05 mmol) in toluene to give I**AB**I as green crystals. Yield: 53 mg (75%). Anal. Calcd for $C_{28}H_{16}N_4O_{12}Ir_4I_2$: C, 20.72; H, 0.99 N, 3.45. Found: C, 20.52; H, 0.78; N, 3.44. IR (Nujol): ν(CO) = 2087 (s), 2071 (m) 2050 (sh), 2041 (s) 2006 (m) cm^{-1}. ^{1}H NMR (C_6D_6 25 °C): δ = 9.65 (dd, 6.3, 1.8 Hz, 1H), 9.52 (dd, 6.3, 2.1 Hz, 1H), 9.48 (dd, 6.3, 1.8 Hz, 1H), 9.21 (dd, 6.3, 1.8 Hz, 1H), 6.56 (m, 2H), 6.53 (m (1H), 6.45 (m, 1H), 6.38 (dd, 8.7, 1.2 Hz, 1H), 6.33 (dd, 8.7, 1.2 Hz, 1H), 6.20 (dd, 8.7, 1.2 Hz, 1H), 6.10 (dd, 8.4, 1.2 Hz, 1H), 5.90 (td, 6.3, 1.2 Hz, 1H), 5.86 (td, 6.3, 1.2 Hz, 1H), 5.74 (m, 2H).

$[Ir_4(\mu\text{-OPy})_4(I)_2(CO)_8]$ (IAAI, 2AA). Addition of solid $[Ir_2(\mu\text{-OPy})_2(CO)_4]$ (68.5 mg, 0.10 mmol) to a toluene solution of diodine (12.7 mg, 0.05 mmol) at room temperature gave immediately a purple solution. The solution was carefully layered with hexane to render blue crystals. The solution was decanted, and the crystals were washed with hexane and vacuum-dried. Yield: 77.1 mg (95%). Anal. Calcd for $C_{28}H_{16}N_4O_{12}Ir_4I_2$: C, 20.72; H, 0.99; N, 3.45. Found: C, 20.94; H, 1.18; N, 3.25. IR (toluene): ν(CO) = 2110 (w), 2093 (s), 2066 (m), 2052 (s), 2027 (w) cm^{-1}. ^{1}H NMR (C_6D_6, 25 °C): δ = 9.52 (dd, 6.6, 1.8 Hz, 4H), 6.47 (ddd, 8.7, 6.6, 1.8 Hz, 4H), 6.26 (dd, 8.7, 1.5 Hz, 4H), 5.73 (td, 6.6, 1.5 Hz, 4H). ^{13}C{^{1}H} NMR (C_6D_6, 25 °C): δ = 175.3, 167.2 (Ir−CO), 165.5 (CO), 152.7, 139.8, 116.7, 115.7.

$[Ir_2(\mu\text{-OPy})_2(I)_2(CO)_4]$ (IAI, 1A). Solid I**AA**I (48.7 mg, 0.030 mmol) was added to a solution of diiodine (7.6 mg, 0.030 mmol) in toluene. The suspension was exposed to the direct sun light to gave an orange solution in 30 min. The solution was evaporated to dryness and the residue extracted with dichloromethane and carefully layered with hexane to render orange crystals. The solution

was decanted, and the solid was washed with cold hexane and vacuum-dried. Yield: 49 mg (87%). Anal. Calcd for $C_{14}H_8N_2O_6I_2Ir_2$: C, 17.92; H, 0.86; N, 2.98. Found: C, 18.17; H, 1.03; N, 2.89. IR (toluene): ν(CO) = 2123 (s), 2095 (m), 2071 (s), 2050 (w) cm^{-1}. ^1H NMR (C_6D_6, 23 °C): δ = 8.90 (ddd, 6.6, 1.8, 0.6 Hz, 2H), 6.34 (ddd, 8.7, 6.6, 1.8 Hz, 2H), 6.22 (ddd, 8.7, 1.2, 0.6 Hz, 2H), 5.61 (td, 6.6, 1.2, 0.6 Hz, 2H).

Oxidation of IABI with Diiodine. The reaction was carried out as described above for the preparation of **1A** to give an equimolar mixture of the **1A** and **1B** isomers of $[Ir_2(\mu\text{-OPy})_2(I)_2(CO)_4]$. The resulting orange microcrystals were separated by hand to obtain pure samples of **1B**. Anal. Calcd for $C_{14}H_8N_2O_6I_2Ir_2$: C, 17.92; H, 0.86; N, 2.98. Found: C, 18.07; H, 0.96; N, 2.91. IR (toluene): ν(CO) = 2123 (s), 2096 (m), 2070 (s) cm^{-1}. ^1H NMR (C_6D_6, 25 °C): δ = 9.30 (dd, 6.6, 1.8 Hz, 2H), 6.35 (ddd, 8.7, 6.6, 1.8 Hz, 2H), 6.19 (dd, 8.7, 1.5 Hz, 2H), 5.67 (td, 6.6, 1.5 Hz, 2H).

Structural determination of complex A: $C_{14}H_8N_2O_6Ir_2$, M_r = 684.62; dark-red needle (0.455 × 0.078 × 0.062 mm); monoclinic, space group *C*2/c; a = 14.1299(15), b = 12.1780(13), c = 19.270(2) Å; β = 105.851(2)°; V = 3189.8(6) $Å^{-3}$; Z = 8; ρ_{calcd} = 2.851 g cm^{-3}; F(000) = 2464; T = 293(2) K; Mo Kα radiation (λ = 0.710 73 Å, μ = 16.703 mm^{-1}). Data were collected with a Bruker SMART APEX CCD diffractometer. Of 18 180 measured reflections (2θ = 4−54°, ω scans 0.3°), 3482 were unique (R_{int} = 0.0631); a multiscan absorption correction was applied (SADABS program)[19] with minimum/maximum transmission factors of 0.040 149/0.129 110. The structure was solved by Patterson and difference Fourier maps and refined using SHELXTL.[20] Final agreement factors were R1 = 0.0319 (2282 observed reflections, $F^2 > 4\sigma(F^2)$) and wR2 = 0.0703 with data/restraints/parameters of 3482/0/218; GOF = 0.854. Hydrogen atoms were included in the model from calculated positions. Atomic scattering factors were used as implemented in the program.[20]

Computational Details. The geometry optimizations of all iridium complexes have been carried out using the DFT formalism with the B3LYP exchange-correlation functional, as implemented in GAUSSIAN-98,[21] except for the precursor dimer **AA** of Figure 1. For all the other systems, the LANL2DZ bases, i.e., full double-ζ bases for first-row atoms and Los Alamos relativistic core potential[22] and valence double-ζ for Ir and I, have been used. The Ir−Ir and Ir−I distances were found to be systematically overestimated by 0.07−0.15 Å with respect to the values obtained from X-ray diffraction (Table 1). A similar deviation was obtained with pure GGA functionals, such as BP86. To investigate the influence of the basis set on the equilibrium distances, the geometry of **1** was reoptimized with polarized basis sets on the heavy atoms including two d-type polarization functions on iodine and one f-type function on iridium. The Ir−Ir and Ir−I distances were reduced by 0.004 and 0.024 Å with respect to the values reported in Table 1. This distance contraction associated with the basis set extension should be taken into account, but it remains modest in view of the computational effort required for optimizing the structure of the largest systems. All calculations reported here were therefore carried out with the standard LANL2DZ bases, except for **AA**. At variance with the oxidized species, the metal−metal bond lengths in the precursor dimer **AA** were found to be sensitive to both the exchange-correlation functional and the quality of the basis set. The geometry optimization of this dimer and the calculation of the energy of the unsupported Ir−Ir bond were therefore carried out using Slater basis sets with the 1999 release of the ADF program.[23] The exchange-correlation functional is the so-called Becke−Perdew/86 (BP86) functional.[24] The atomic basis sets used in the present calculations are of triple-ζ + polarization quality for the valence shells. They are referred to in the User's Guide as TZP for nonmetal atoms and TZ2P for Ir. These basis sets are to be used in conjunction with frozen cores (He cores for first-row atoms; Kr core for iodine, and Xe core for iridium) described with one Slater orbital for each atomic shell and with the zero order regular approximation (ZORA)[25] to the relativistic effects.

Acknowledgment. All calculations have been carried out at the IDRIS computer center (Orsay, France), through a grant of computer time from the CNRS, and at the CURRI (ULP, Strasbourg, France). We are also pleased to acknowledge support from the GdR DFT and from Ministerio de Ciencia y Tecnología (McyT(DGI)/FEDER) Projects BQU2002-0074 and BQU-2003-05412.

Supporting Information Available: An X-ray crystallographic file, in CIF format, containing full details of the structural analyses of complex **A** and a file containing (i) a comprehensive diagram displaying the enthalpies of formation calculated for $I-[Ir_2(\mu\text{-OPy})_2(CO)_4]_n-I$ (n = 1−4) (Figure S1) and (ii) the Cartesian coordinates of all molecules after geometry optimization. This material is available free of charge via the Internet at http://pubs.acs.org.

IC050419W

(19) *SAINTPLUS program*, v. 6.28; Bruker AXS: Madison, WI, 2001. Blessing, R. H. *Acta Crystallogr., Sect. A* **1995**, 51, 33. This was implemented in the following: *SADABS: Area-detector absorption correction*, v. 2.03; Bruker-AXS: Madison, WI, 2002.

(20) *TL Package*, v. 6.10; Bruker-AXS: Madison, WI, 2000. Sheldrick, G. M. *SHELXS-86 and SHELXL-97*; University of Göttingen: Göttingen, Germany, 1997.

(21) Frisch, M. J.; et al. *Gaussian 98*, revision A.6; Gaussian, Inc.: Pittsburgh, PA, 1998.

(22) (a) Hay, P. J.; Wadt, W. R. *J. Chem. Phys.* **1985**, *82*, 270. (b) Wadt, W. R.; Hay, P. J. *J. Chem. Phys.* **1985**, *82*, 284. (c) Hay, P. J.; Wadt, W. R. *J. Chem. Phys.* **1985**, *82*, 299.

(23) (a) *Amsterdam Density Functional (ADF), User's Guide*, release 1999; Chemistry Department, Vrije Universiteit: Amsterdam, The Netherlands, 1999. (b) Baerends, E.-J.; Ellis, D. E.; Ros, P. *Chem. Phys.* **1973**, *2*, 41. (c) te Velde, G.; Baerends, E.-J. *Comput. Phys.* **1992**, *99*, 84. (d) Fonseca-Guerra, C.; Visser, O.; Snijders, J. G.; te Velde, G.; Baerends, E.-J. *Methods and Techniques in Computational Chemistry: METECC-95*; Clementi, E., Corongiu, G., Eds.; STEF: Cagliari, Italy, 1995; pp 305−395.

(24) (a) Becke, A. D. *J. Chem. Phys.* **1993**, *98*, 5648. (b) Perdew, J. P. *Phys. Rev.* **1986**, *B33*, 8882; *B34*, 7406.

(25) (a) van Lenthe, E.; Baerends, E.-J.; Snijders, J. *J. Chem. Phys.* **1993**, *99*, 4597. (b) van Lenthe, E.; Baerends, E.-J.; Snijders, J. *J. Chem. Phys.* **1996**, *105*, 6505.